



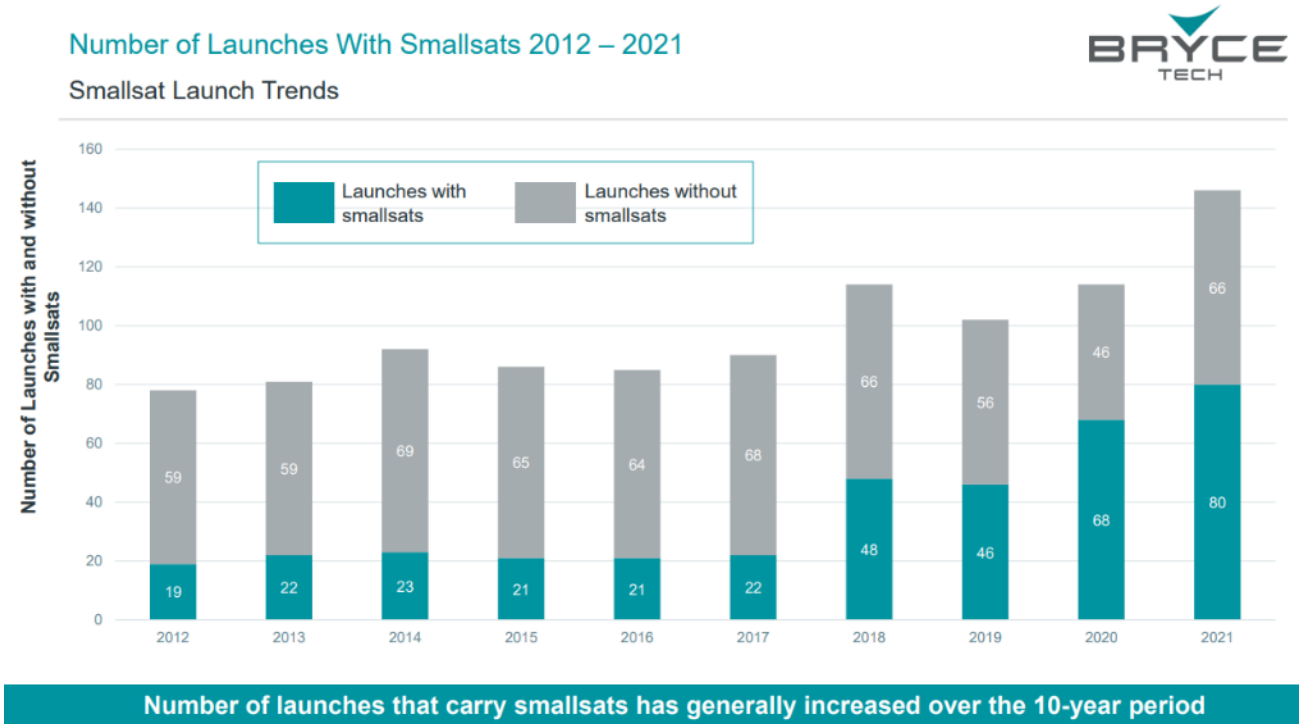
Development of Mirror Target Calibration for Multiple Optical Satellite Data

Masahiko Nagai

Center for Research and Application of Satellite Remote Sensing (YUCARS)
Yamaguchi University

Introduction

- Since the advent of the New Space Ecosystem, microsattellites have been increasing and their commercial use in various application is becoming more common.



Ref: https://brycetek.com/reports/report-documents/Bryce_Smallsats_2022.pdf

- Moreover, there will be a greater number of microsattellites for earth observation in the future.
- Each satellite sensors have different specifications which resulted into different quality and visualization.
- Therefore, sensor and data calibration is an important step for precise and accurate remote sensing measurement.

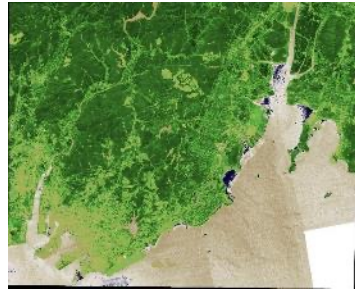
Introduction

- Different sensors and environmental conditions affect to the quality of satellite images.

Normalized difference vegetation index (NDVI)



2020-03-20_Planet



2020-03-23_GRUS



2020-03-24_Planet



2020-03-29_Planet



2020-04-02_Planet



2020-04-04_GRUS



2020-04-07_Planet



2020-04-15_GRUS



2020-04-15_Planet



2020-04-16_GRUS



2020-04-25_Planet



2020-04-29_Planet

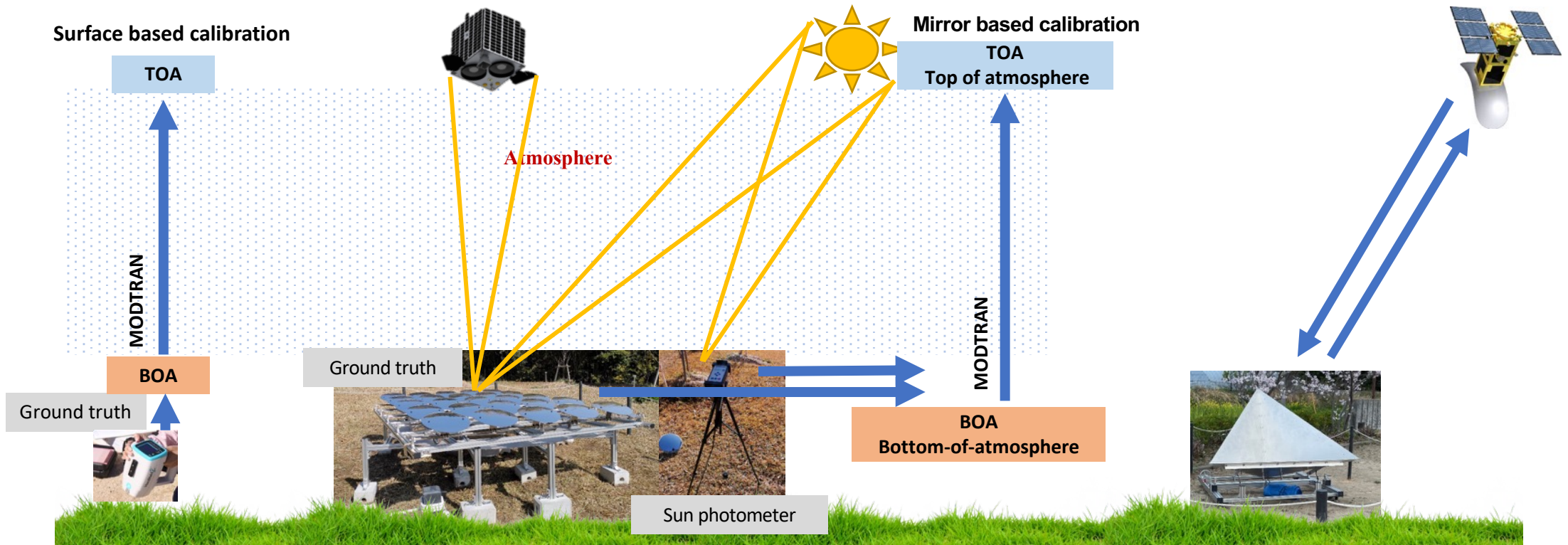
- To utilize multi-sensor satellite images for data application, the radiometric calibration is very crucial for evaluating quality and calibrating satellite data to be more precise and well harmonize for real world applications.

Introduction:

Yamaguchi Univ. builds calibration sites for current and upcoming new microsattellites.

- Selected/constructed optical satellite data calibration sites based on
 - Surface reflectance measurements
 - Ground point source-mirror reflectors
- Constructed SAR satellite data calibration site
 - Corner reflector

Data calibration
Data utilization
(Disaster,, Infrastructure
and environment
monitoring)

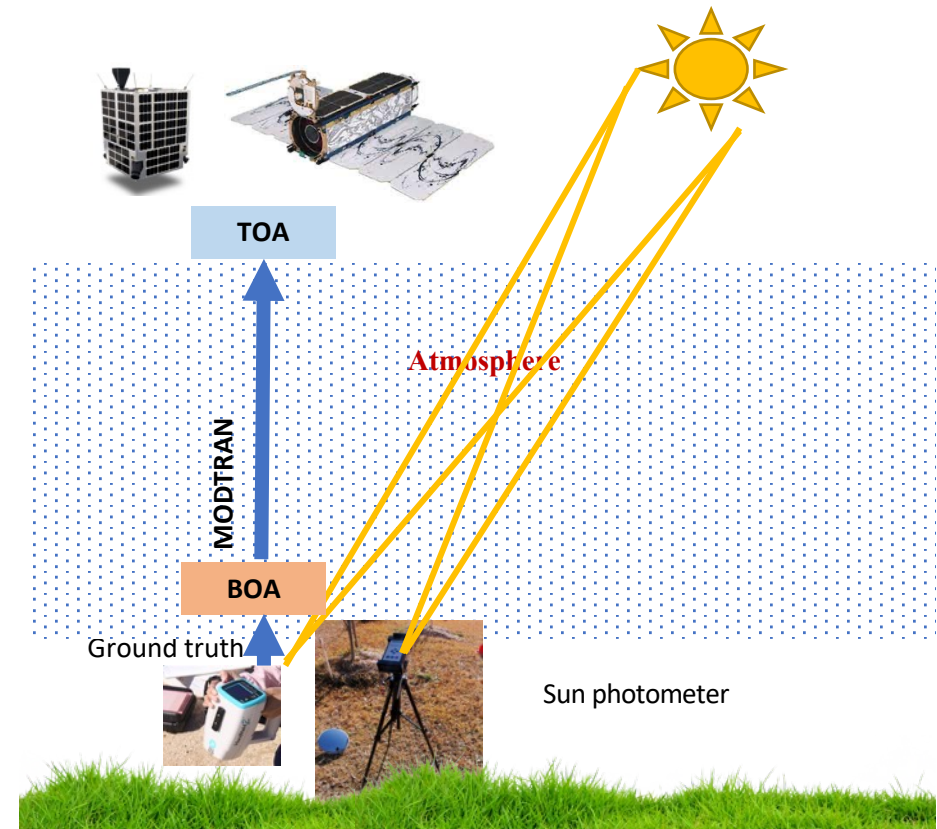


Introduction and objective

- In previous studies, radiometric calibration has been successfully performed using artificial objects such as permanent back and white area.
- In case of conventional calibration site such as permanent back and white area, it is difficult in Japan because un-utilized area is limited.

Objective

- Yamaguchi Univ. has established a calibration site based on convex mirror array at Ube city, Yamaguchi Prefecture, Japan.
- The main goal of the project is to make better quality, better accuracy, better harmonization of multi-sensor satellite, especially constellation satellites.





Data used

Satellite constellation

5 GRUS
satellites

~130
PlanetScope
satellites

5 August 2021

GRUS1A

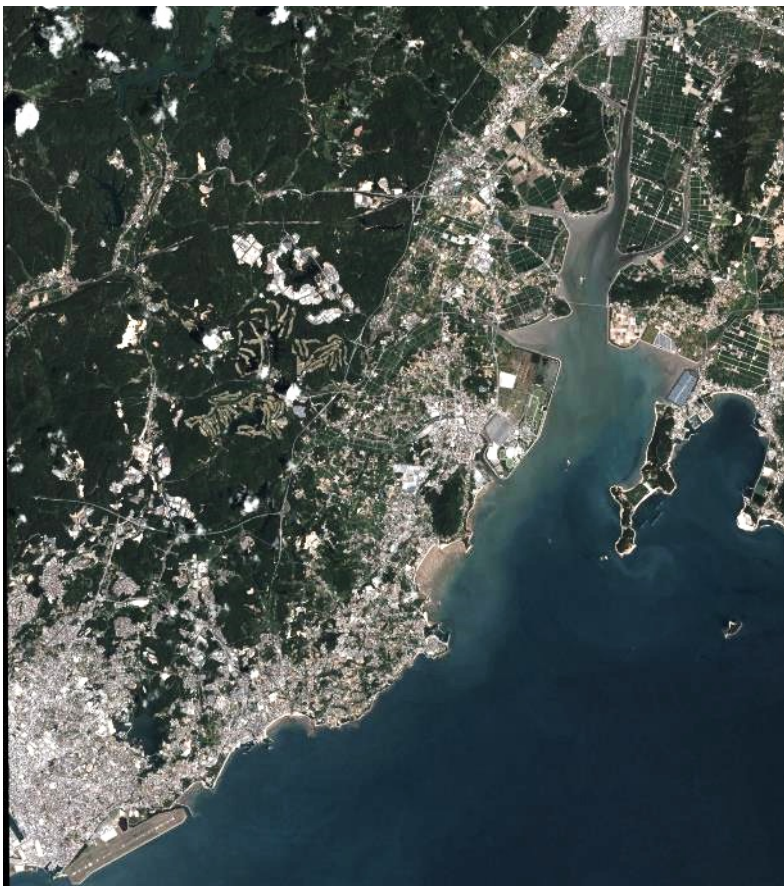
PlanetScope PS2

PlanetScope PSB.SD

| | | |
|-------------------|---------------|------------|
| Spectral bands | Panchromatic | 450-900 nm |
| | Blue | 450-505 nm |
| | Green | 515-585 nm |
| | Red | 620-685 nm |
| | Red Edge | 705-745 nm |
| | Near Infrared | 770-900 nm |
| | Swath | 57+ Km |
| Ground resolution | Panchromatic | 2.5 m |
| | Multispectral | 5.0 m |

| Instrument | PS2 | PSB.SD |
|----------------|---|---|
| Spectral Bands | Blue: 455 - 515 nm Green: 500 - 590 nm Red: 590 - 670 nm NIR: 780 - 860 nm | Blue: 465 - 515 nm Green: 513 - 549 nm Red: 650 - 680 nm Red-Edge: 697 - 713 nm NIR: 845 - 885 nm (8-band will be released in the future) |
| Resolution | 3.125 m | |

True color composite



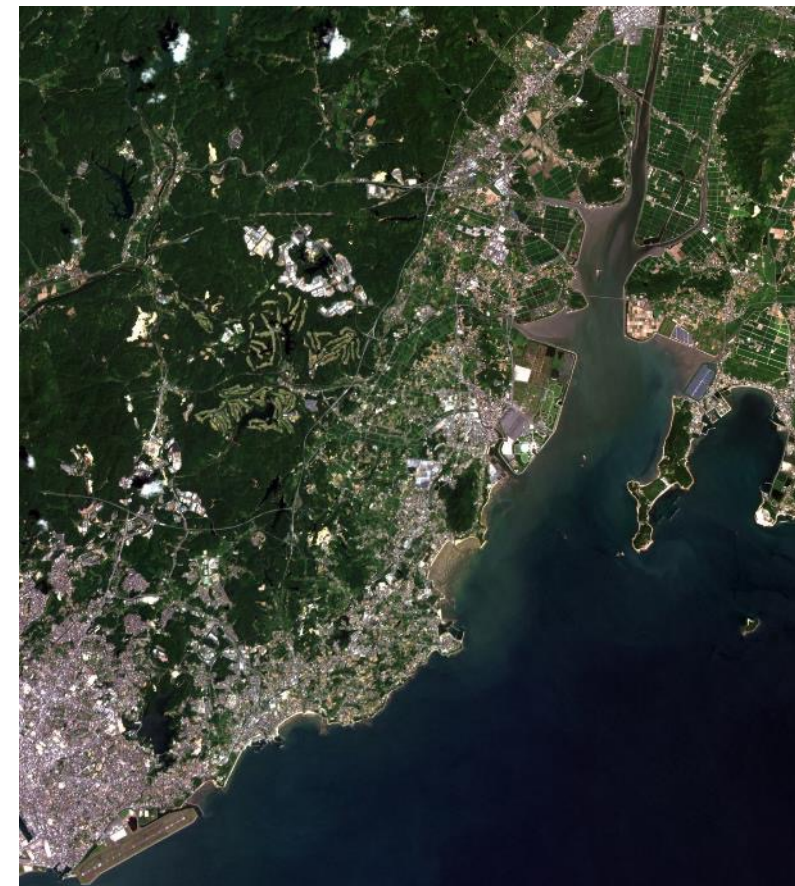
PlanetScope PS2

Date: 2022-08-05
Local Time: 10:34 am.



PlanetScope PSB.SD

Date: 2022-08-05
Local Time: 10:11 am.



GRUS1

Date: 2022-08-05
Local Time: 10:47 am.

Ground data collection

- Surface reflectance by Spectroradiometer
 - HandHeld 2
- Atmospheric measurements by Sunphotometer
 - MICROTOPS II 540
- Location of the measurements by GPS
 - Garmin etrex20xJ
 - Garmin GPS73 and Ichimill GPS



HandHeld 2



Ichimill GPS
(3 cm resolution)



Garmin etrex20xJ



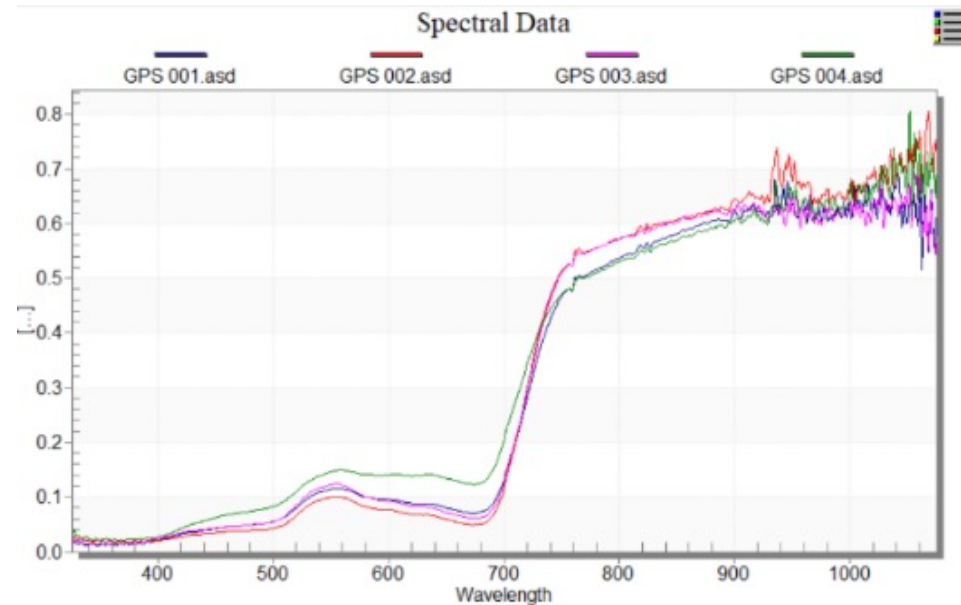
Garmin GPS73



Microtops II 540



Spectroradiometer



GRUS1A

| File Name | RED | RED_Edge | GREEN | BLUE | NIR |
|-----------|----------|----------|----------|----------|----------|
| 001.asd. | 0.079784 | 0.313083 | 0.103196 | 0.049014 | 0.565574 |
| 002.asd. | 0.058683 | 0.334836 | 0.087877 | 0.038922 | 0.595021 |
| 003.asd. | 0.071731 | 0.33167 | 0.108437 | 0.049056 | 0.591496 |
| 004.asd. | 0.132771 | 0.3617 | 0.136567 | 0.073323 | 0.556273 |

PlanetScope PS2

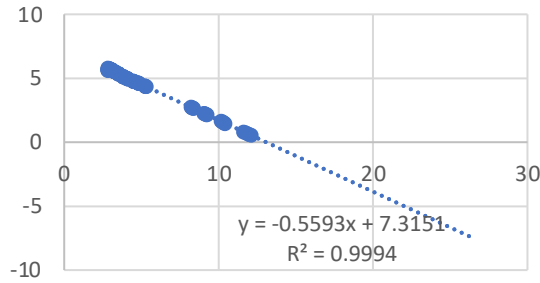
| File Name | RED | GREEN | BLUE | NIR |
|-----------|----------|----------|----------|----------|
| 001.asd. | 0.086335 | 0.095922 | 0.051939 | 0.554396 |
| 002.asd. | 0.066028 | 0.08073 | 0.041078 | 0.586623 |
| 003.asd. | 0.08049 | 0.100042 | 0.052045 | 0.583822 |
| 004.asd. | 0.136882 | 0.129038 | 0.077406 | 0.545775 |

PlanetScope PSB.SD

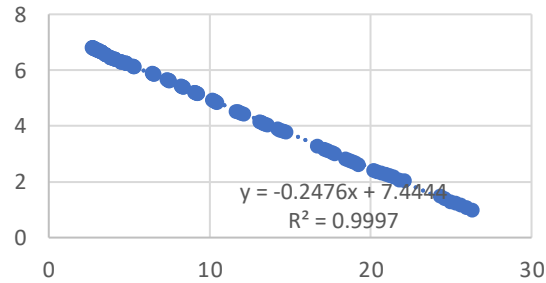
| File Name | RED | GREEN | BLUE | NIR |
|-----------|----------|----------|----------|----------|
| 001.asd. | 0.074076 | 0.109549 | 0.053835 | 0.59422 |
| 002.asd. | 0.052802 | 0.093105 | 0.042445 | 0.616047 |
| 003.asd. | 0.064865 | 0.113923 | 0.053947 | 0.612558 |
| 004.asd. | 0.127271 | 0.145639 | 0.080133 | 0.581955 |

Calibration of Sun photometer Microtops II

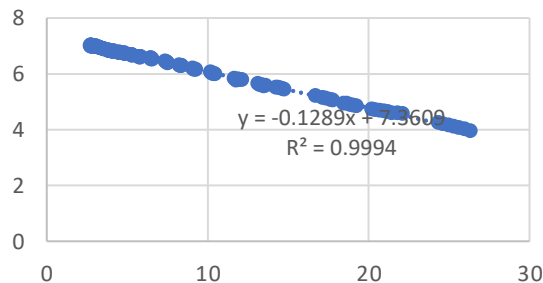
SIG380



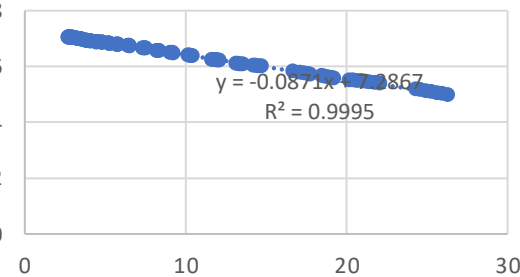
SIG500



SIG675



SIG870



Angstrom exponent

An Aerosol Optical Properties can be determined by Angstrom coefficient.

$$\alpha = -\frac{\ln(\tau_{0.5}) - \ln(\tau_{0.87})}{\ln(0.5) - \ln(0.87)}$$

Kirara 2021/08/05

Sig500 = 1478.84

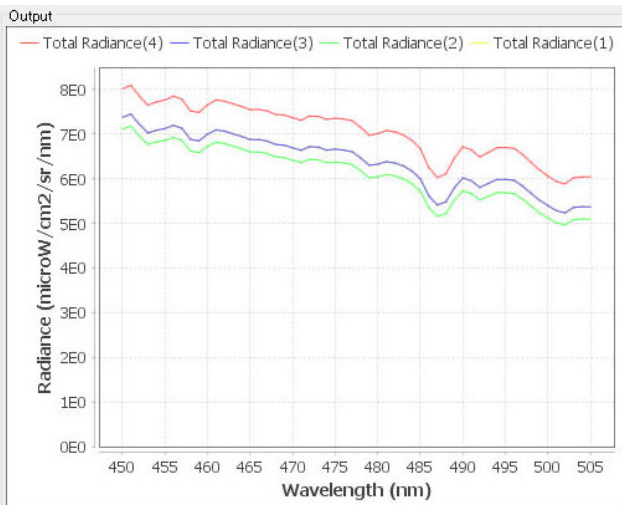
Sig870 = 1397.49

Angstrom exponent = 0.102151556

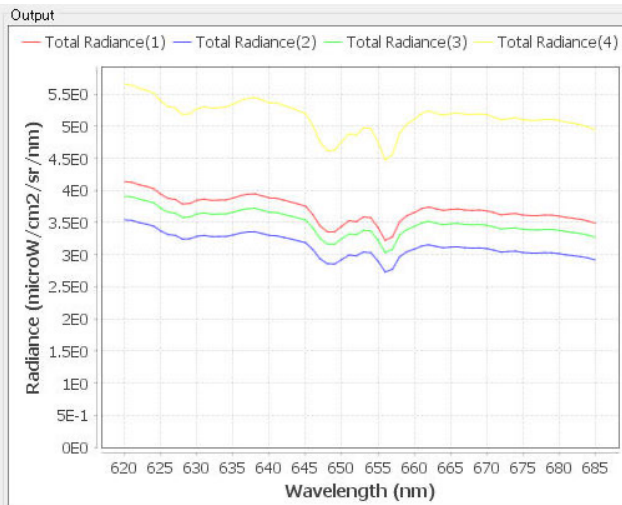
| Band name | Langley plot line | The extraterrestrial constant V_0 | |
|-----------|-------------------------|-------------------------------------|----------------|
| 380nm | $y = -0.5593x + 7.3151$ | 7.3151 | $R^2 = 0.9994$ |
| 500nm | $y = -0.2476x + 7.4444$ | 7.4444 | $R^2 = 0.9997$ |
| 675nm | $y = -0.1289x + 7.3609$ | 7.3609 | $R^2 = 0.9994$ |
| 870nm | $y = -0.0871x + 7.2867$ | 7.2867 | $R^2 = 0.9995$ |
| 1020nm | $y = -0.0775x + 7.3733$ | 7.3733 | $R^2 = 0.9972$ |

MODTRAN output sample (TOA Radiance)

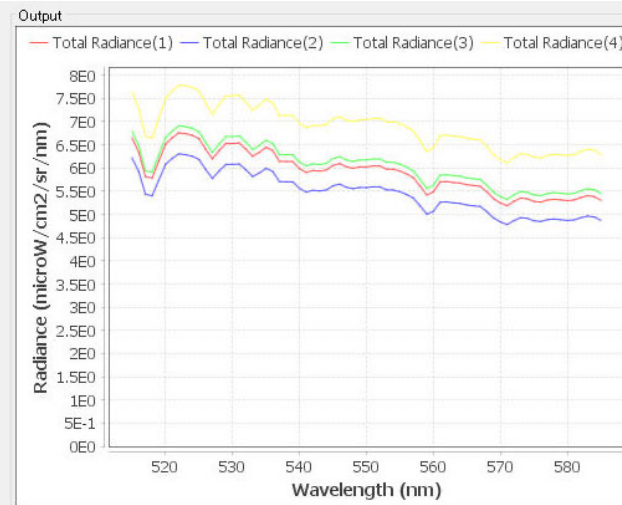
Blue



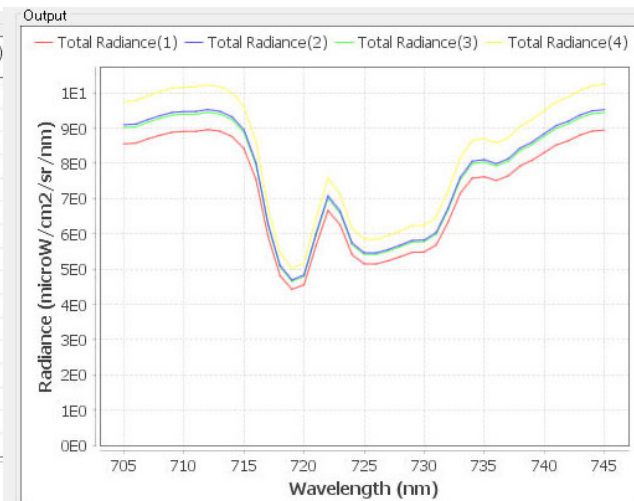
Green



Red

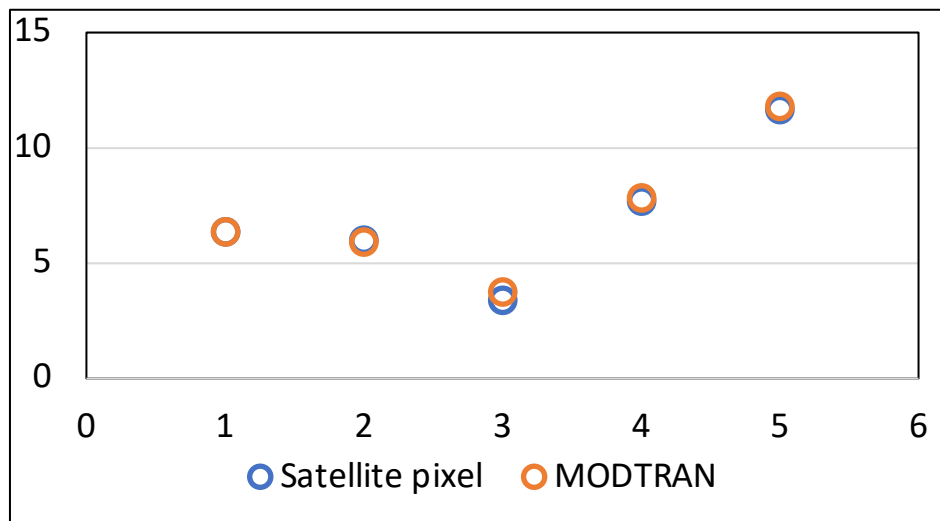


NIR



GRUS-1A

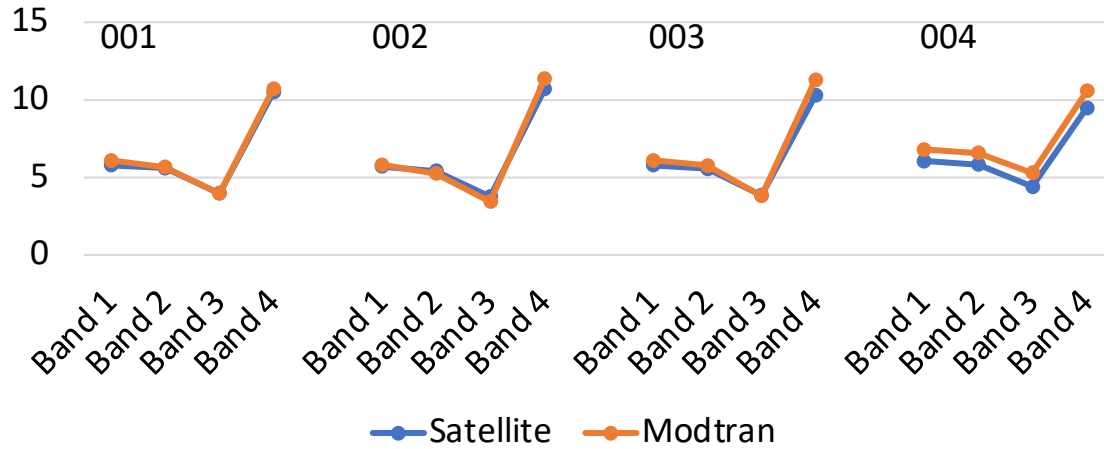
Comparison of TOA radiance and reflectance estimated from MODTRAN and satellite images



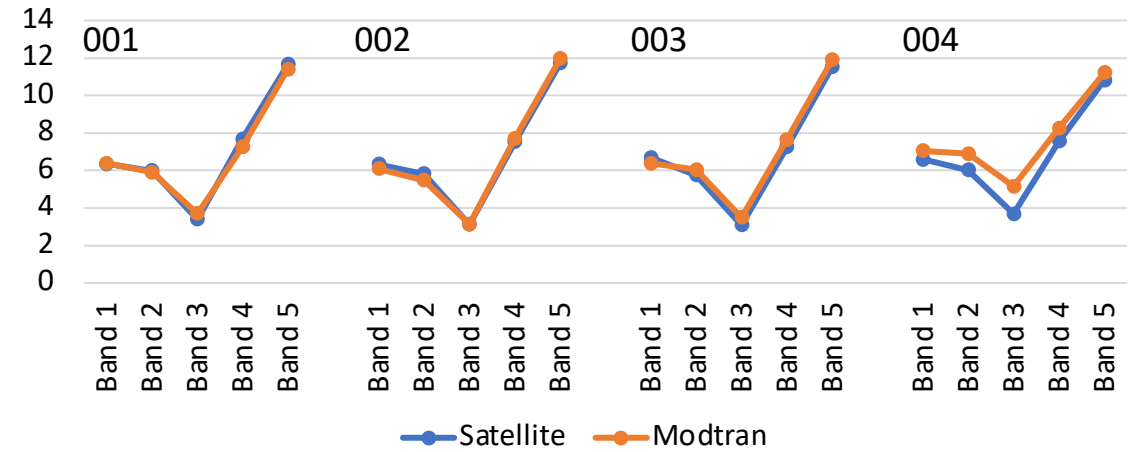
| | Band 1 | Band 2 | Band 3 | Band 4 | Band 5 |
|--------------------------------------|--------|--------|---------|---------|---------|
| Satellite pixel | 6.354 | 5.991 | 3.395 | 7.686 | 11.659 |
| Modtran simulation | 6.349 | 5.912 | 3.746 | 7.811 | 11.793 |
| Difference (Satellite - Modtran) | 0.005 | 0.079 | -0.351 | -0.125 | -0.134 |
| Difference (%) (Difference/ Modtran) | 0.077% | 1.338% | -9.372% | -1.604% | -1.133% |

Comparison of simulated MODTRAN and Satellites (TOA)

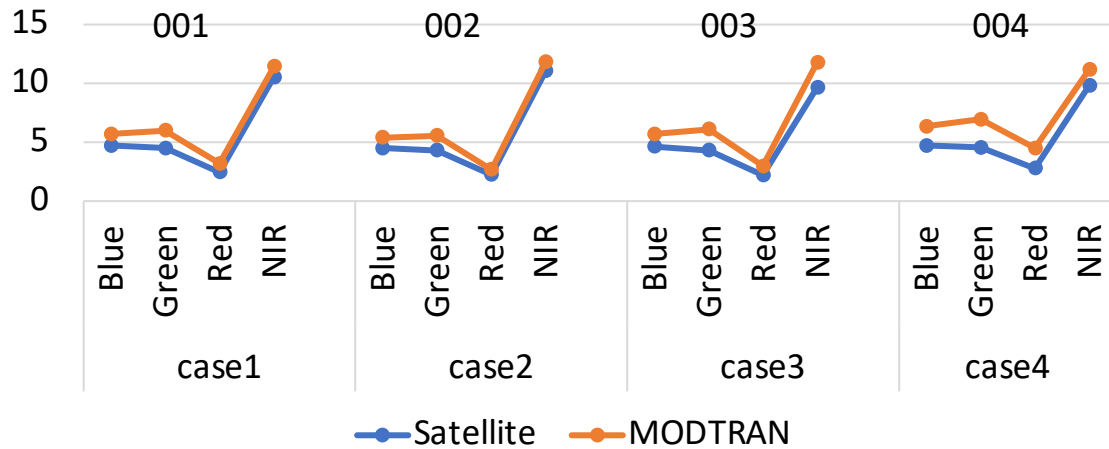
PS2 Radiance



GRUS1A Radiance



PSB.SD Radiance



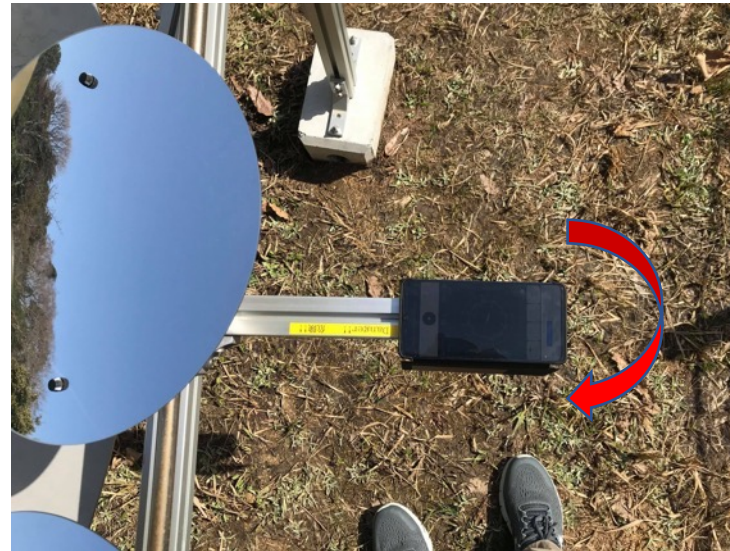
Characteristics of YUCARS's Mirror Array



In accordance to the YUCARS's tasking and scheduling for satellite observation, the mirror reflectors have been set up by adjusting a precise azimuth and tilt angles to get maximum reflectance from the mirrors.



A key for tilt angle adjustment

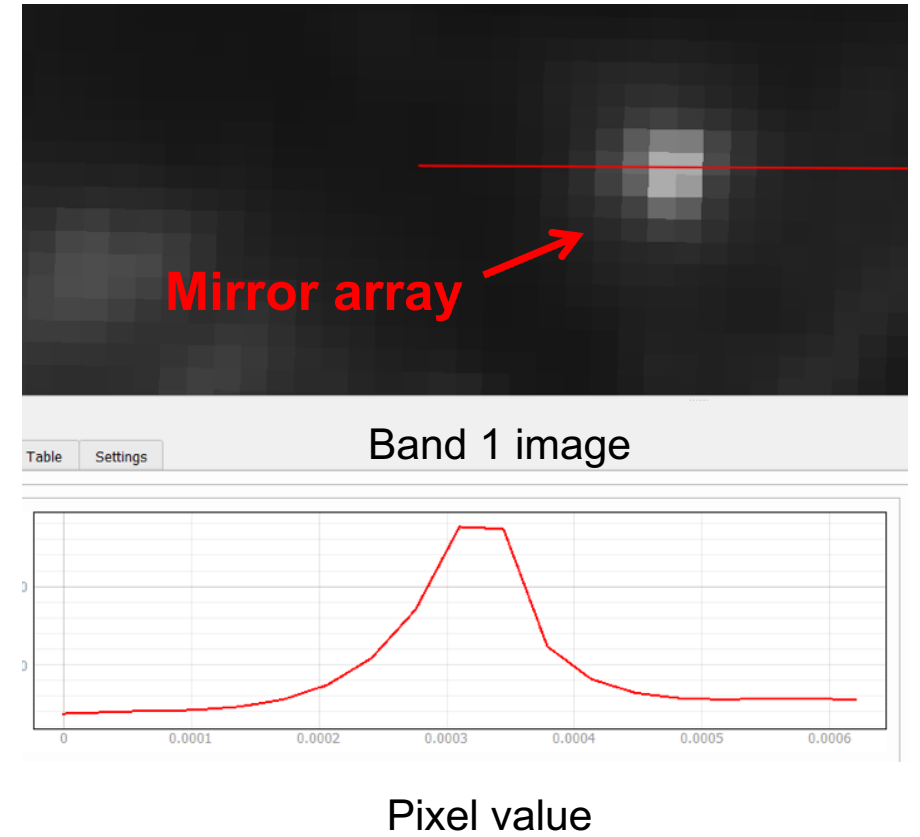


A key for azimuth angle adjustment



Mirror reflectors after adjustment

Observation of Mirror Array by GRUS-1A



2021-02-22

Image of Mirror Array

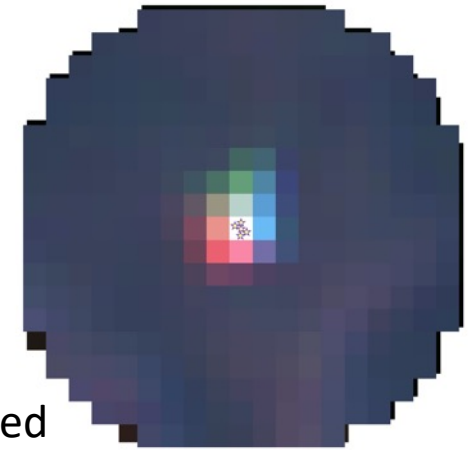
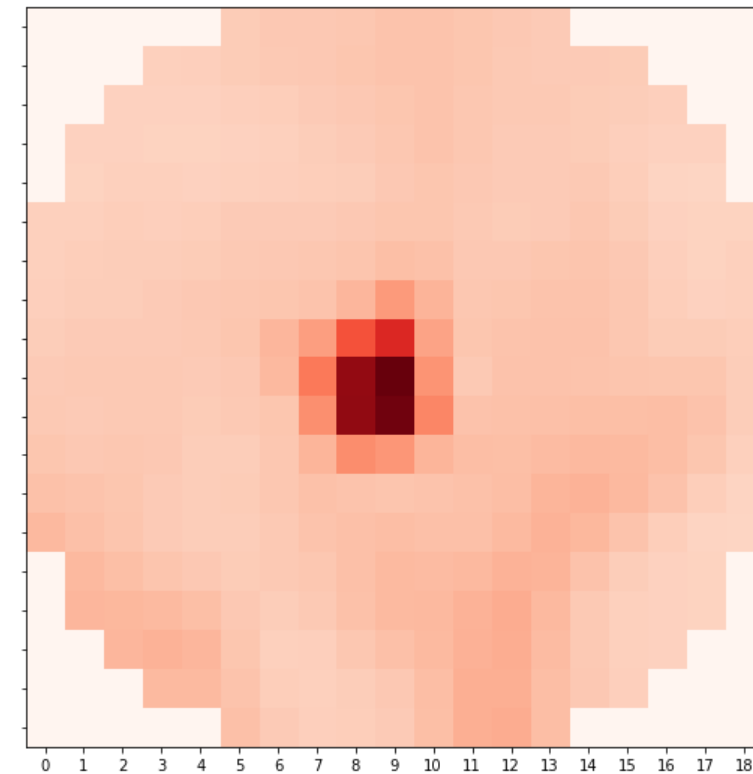
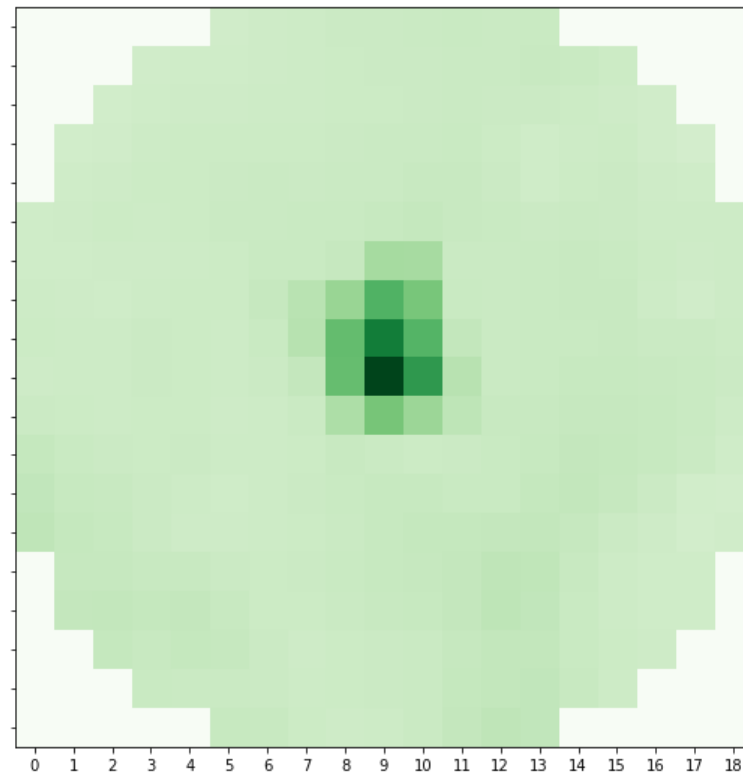
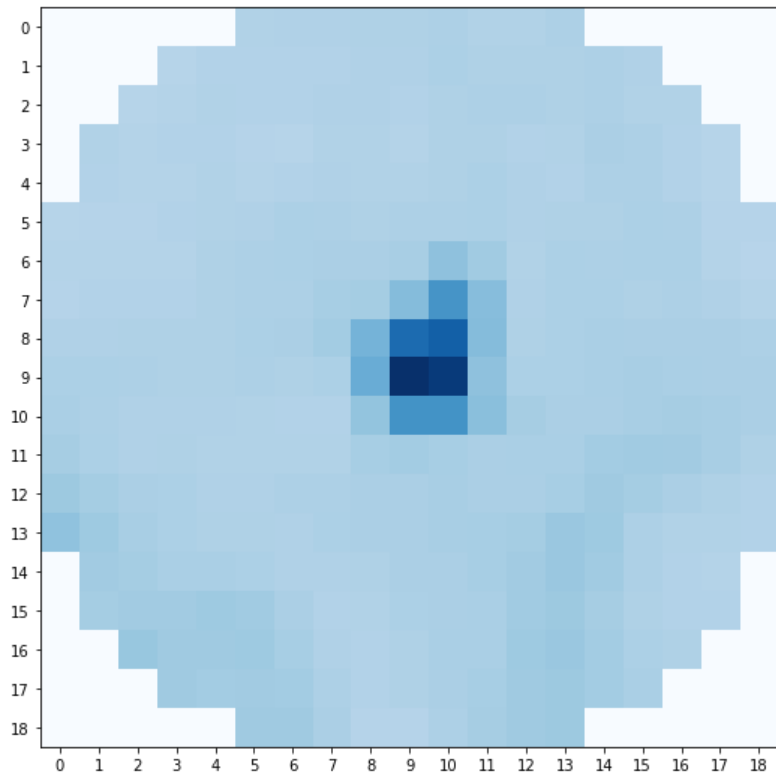


Image chip used

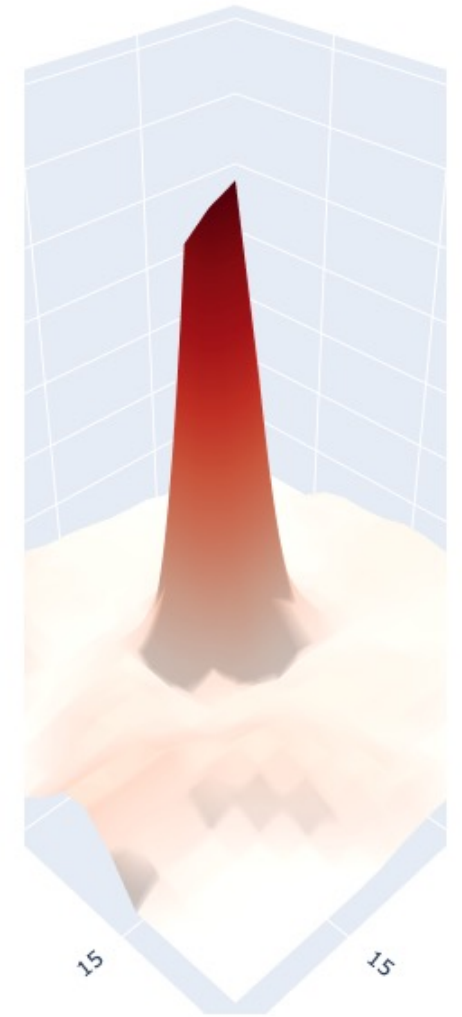
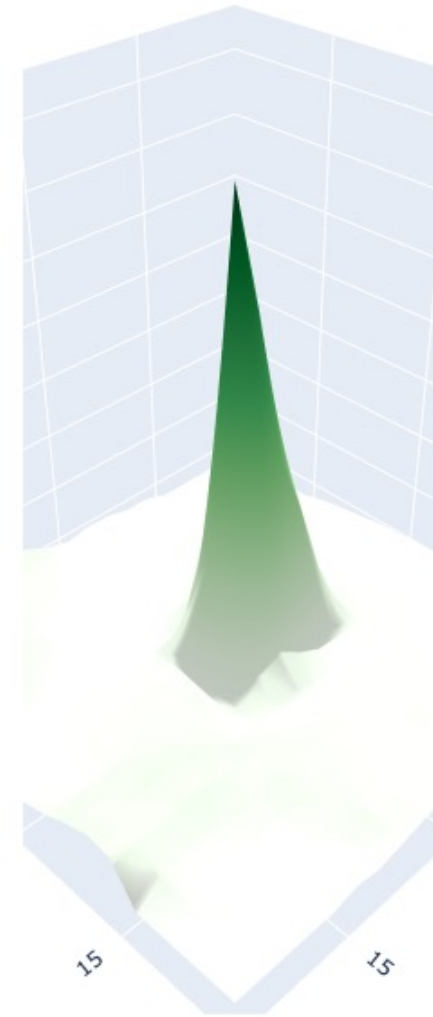
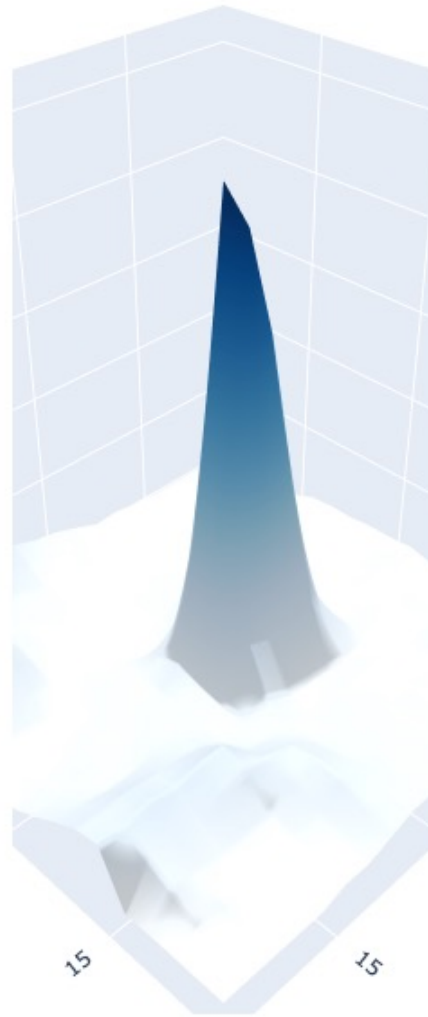


Energy Spread of Various Bands

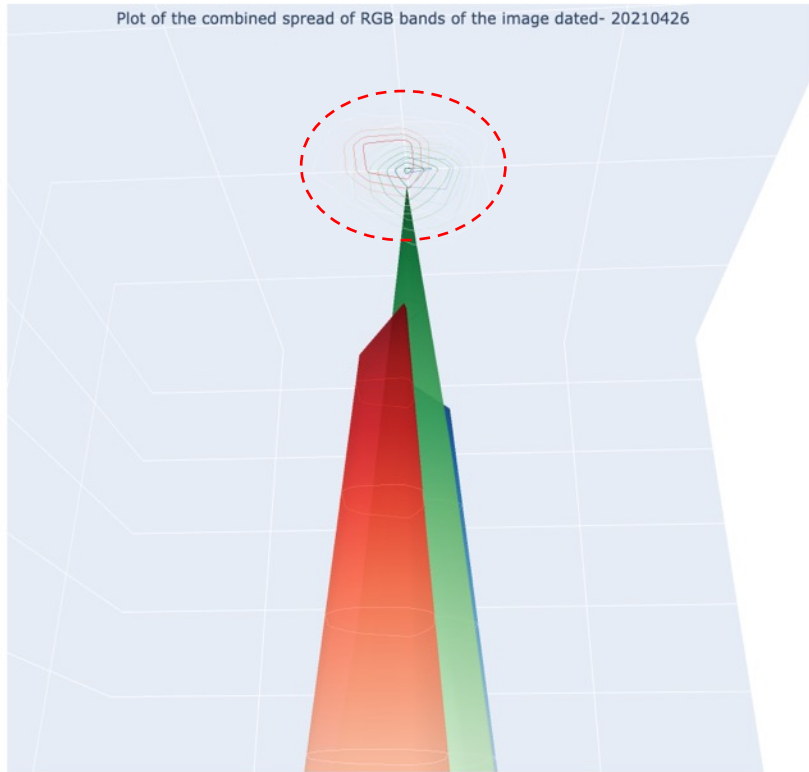
Plots of the separate bands of the GRUS dated - 20210426

Energy distribution of each band is better as only single peak is visible in the plot.

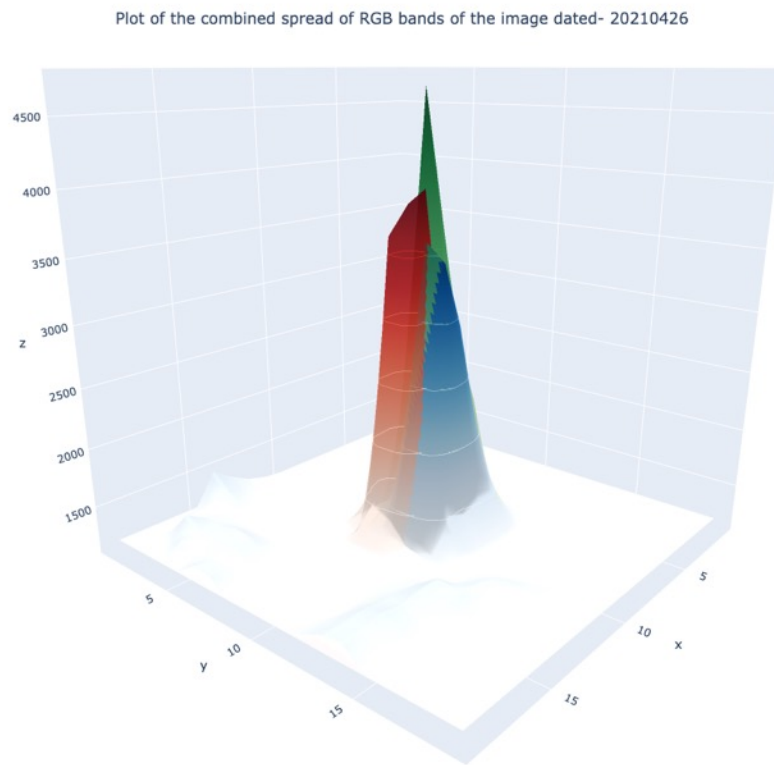
Among all three bands, Green band performance is best, while the red band has worst.



Energy Spread of Plot of Bands Together



Contour lines



Side perspective

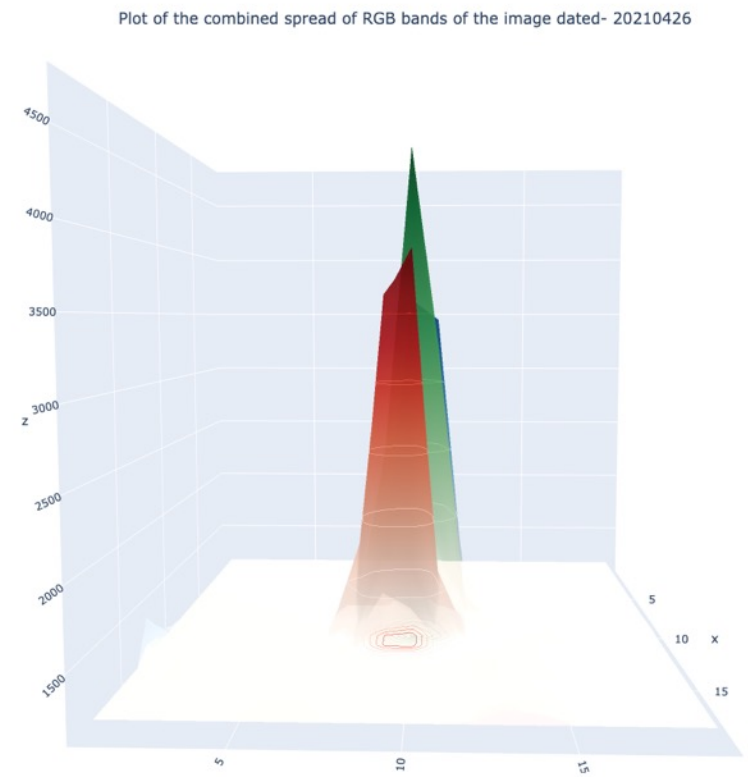
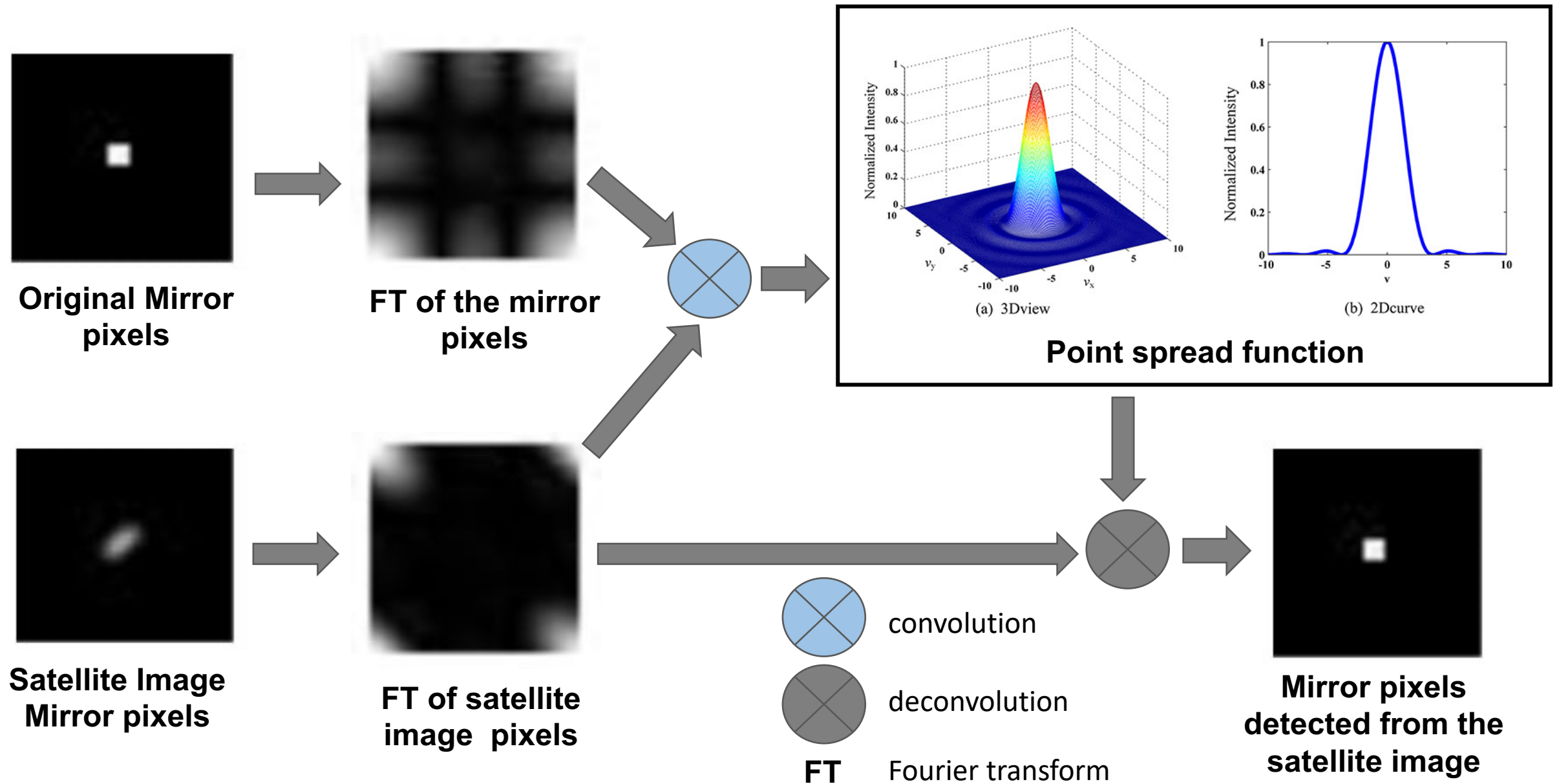


Image perspective

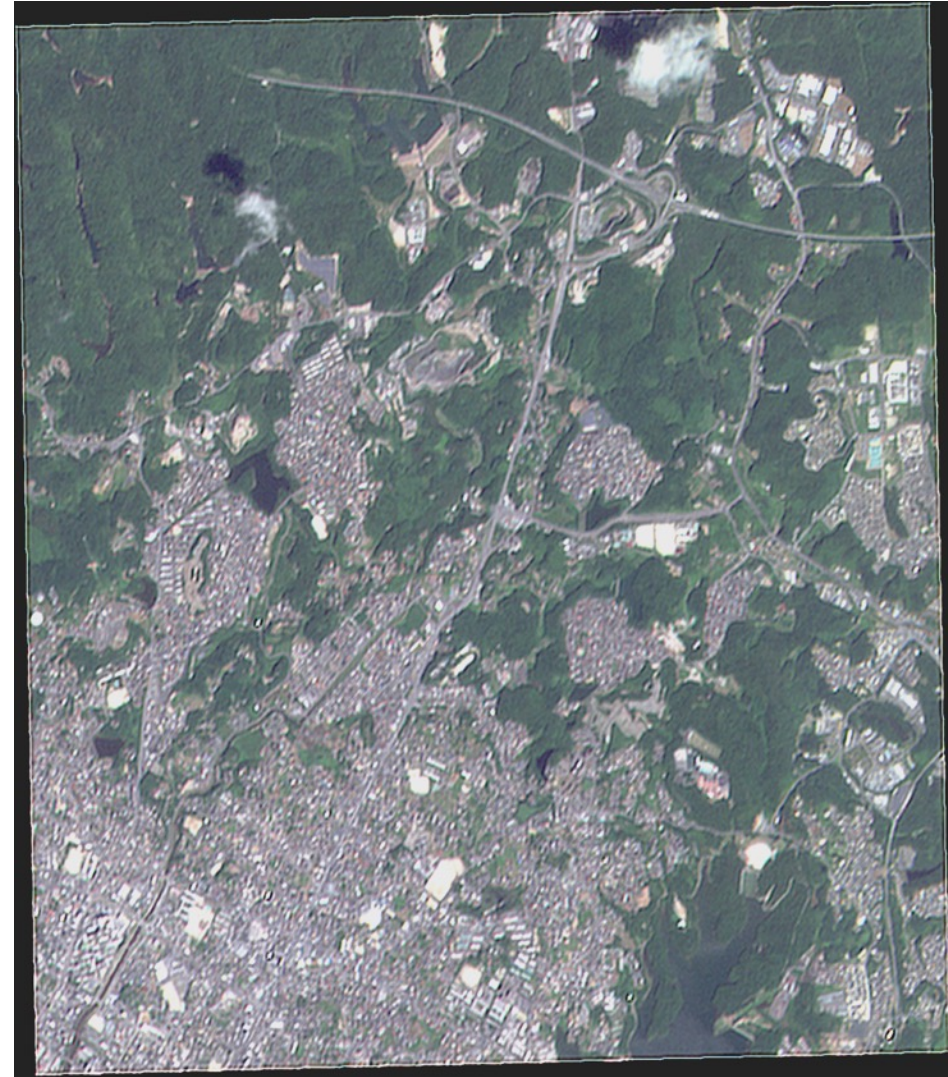
Concept of PSF (Point Spread Function) Calibration



PSF for Image Reconstruction by Removing Distortions




The original RGB image
(blurred source image



The blind deconvolved image using the PSF
(deblurred image)

Former Machine Learning for Satellite image




GRUS-1 Image

Training Data set generated from GRUS-1

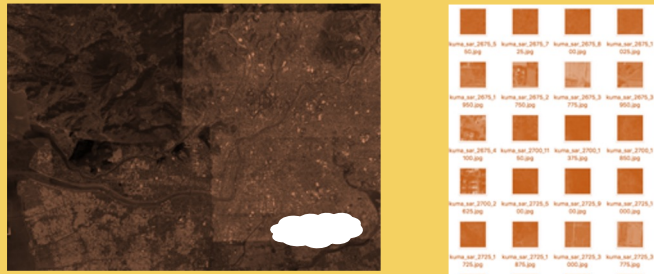
Machine Learning

Model A



Object detection by GRUS-1

This panel illustrates the machine learning pipeline for GRUS-1 satellite imagery. It starts with a satellite image of a landscape with a white cloud mask. A training data set is generated from this image, consisting of a grid of small satellite image patches with corresponding bounding boxes. The process then moves to machine learning, resulting in Model A. The final output is an object detection map where the cloud mask is black and other objects are outlined in cyan.




PlanetScope Image

Training Data set generated from PlanetScope

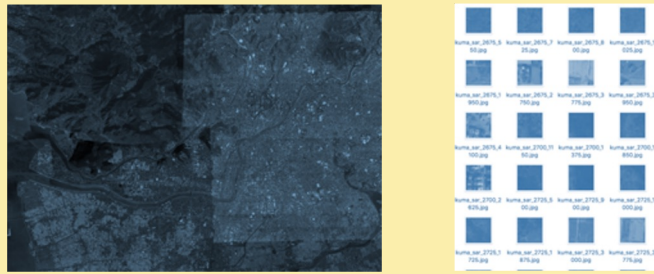
Machine Learning

Model B



Object detection by PlanetScope

This panel illustrates the machine learning pipeline for PlanetScope satellite imagery. It starts with a satellite image of a landscape with a white cloud mask. A training data set is generated from this image, consisting of a grid of small satellite image patches with corresponding bounding boxes. The process then moves to machine learning, resulting in Model B. The final output is an object detection map where the cloud mask is black and other objects are outlined in cyan.




Formosat-5 Image

Training Data set generated from Formosat-5

Machine Learning

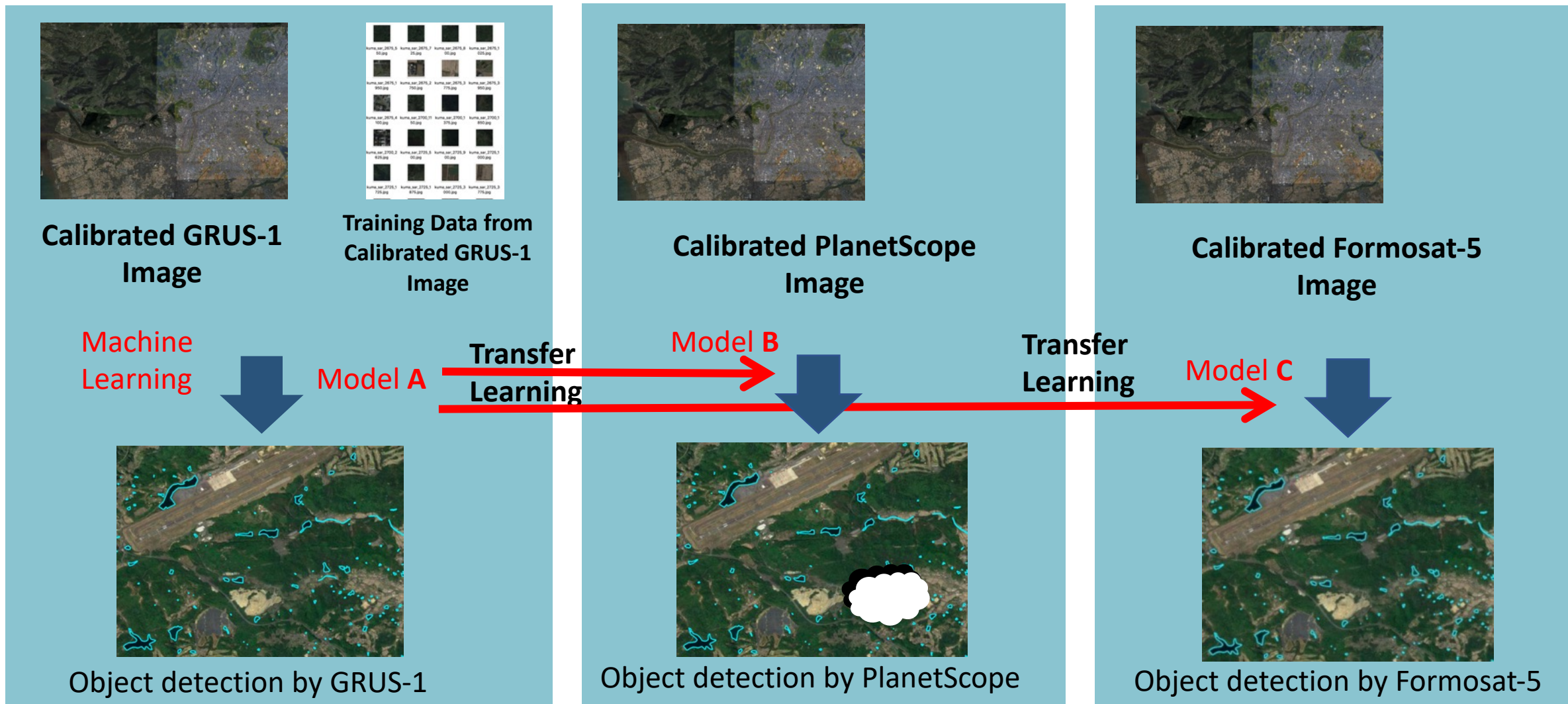
Model C



Object detection by Formosat-5

This panel illustrates the machine learning pipeline for Formosat-5 satellite imagery. It starts with a satellite image of a landscape with a white cloud mask. A training data set is generated from this image, consisting of a grid of small satellite image patches with corresponding bounding boxes. The process then moves to machine learning, resulting in Model C. The final output is an object detection map where the cloud mask is black and other objects are outlined in cyan.

Transfer Learning with Calibrated Satellite image



Summary

1. Yamaguchi Univ. demonstrates **convex mirrors calibration** sites, which is called **mirror array target**.
2. This site consisting of **mirror array** as point source has been established and it allows to apply mirror technology different than traditional method.
3. The analysis shows **radiometric performance** and spread of reflected energy from the mirror center for the individual bands.
4. This site is used to construct point spread function (PSF) which has a strong potential **to improve image quality** by deblurring and defocusing techniques.

Observation of Mirror Array



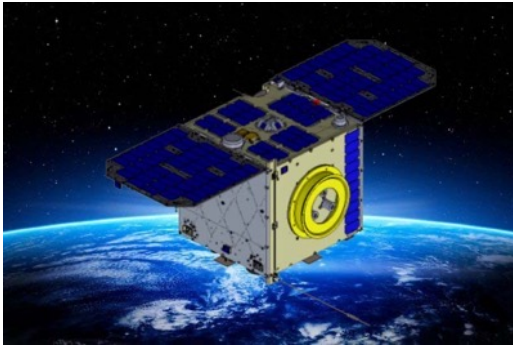
AXELSPACE



Observation of Mirror Array by Cartosat 2E



Next Observation Plan for Mirror Array



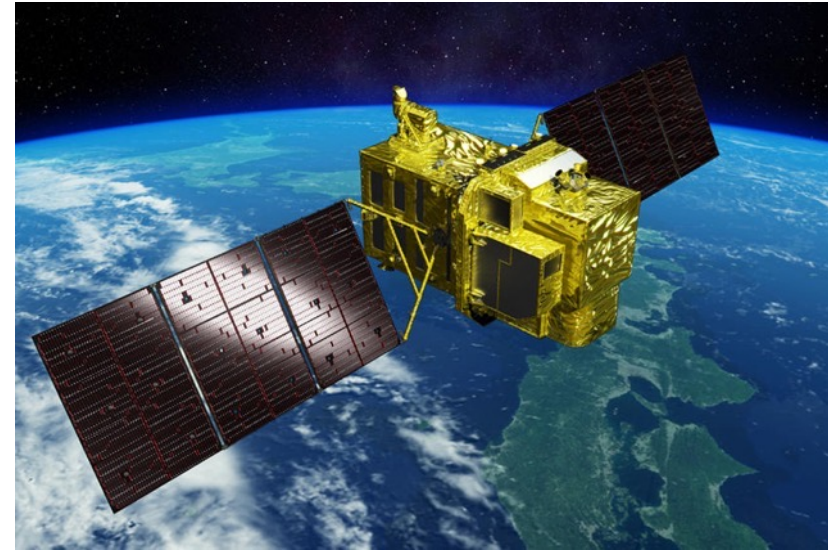
DIWATA-2



**Philippine
Space
Agency**



October 20 Capture – SMI




ALOS-3

Research
Announcement
on the Earth
Observations:
EO-RA3



NSPO

An aerial photograph of a coastal city, likely Yamaguchi, Japan, showing a mix of greenery, urban buildings, and a coastline with a bay. A large white semi-transparent banner is overlaid across the center of the image, containing the text "Thank you for your kind attention".

**Thank you for
your kind attention**